Environmental Research 206 (2022) 112280

Contents lists available at ScienceDirect

Environmental Research

journal homepage: www.elsevier.com/locate/envres

Coal fly ash supported $CoFe_2O_4$ nanocomposites: Synergetic Fenton-like and photocatalytic degradation of methylene blue

Nimra Nadeem [a], Muhammad Yaseen [b], Zulfiqar Ahmad Rehan [c], Muhammad Zahid [a,*], Rana Abdul Shakoor [d], Asim Jilani [e,**], Javed Iqbal [e], Shahid Rasul [f], Imran Shahid [g]

[a] Department of Chemistry, University of Agriculture Faisalabad, Pakistan
[b] Department of Physics, University of Agriculture Faisalabad, Pakistan
[c] Department of Polymer Engineering, National Textile University Faisalabad, Pakistan
[d] Center for Advanced Materials (CAM), Qatar University, P.O. Box 2713, Doha, Qatar
[e] Center of Nanotechnology, King Abdulaziz University, Jeddah, Saudi Arabia
[f] Department of Mechanical and Construction Engineering, Northumbria University, UK
[g] Environmental Science Centre, Qatar University, Doha, P.O. Box 2713, Qatar

ARTICLE INFO

Keywords:
CFA nanocomposites
Photo-Fenton process
Heterogeneous photocatalysis
Response surface methodology
Wastewater treatment
Metal ferrites

ABSTRACT

Rapid industrialization is causing a serious threat for the environment. Therefore, this research was aimed in developing ceramic cobalt ferrite ($CoFe_2O_4$) nanocomposite photocatalyst coated with coal fly ash (CFA-$CoFe_2O_4$) using facile hydrothermal synthesis route and their applications against methylene blue. The pristine cobalt ferrite photocatalyst was also prepared, characterized, and applied for efficiency comparison. Prepared photocatalyst were characterized by X-ray diffraction (XRD), fourier transformed infrared (FTIR) spectroscopy, X-ray photoelectron spectroscopy (XPS), and scanning electron microscopy with energy dispersive spectroscopy (SEM/EDS). Optical response of catalysts was check using photoluminescence spectroscopy (PL). pH drift method was used for the surface charge characteristics of the material under acidic and basic conditions of solution pH. The photocatalytic degradation potential of all the materials were determined under ultra-violet irradiations. The influencing reaction parameters like pH, catalyst dose, oxidant dose, dye concentration, and irradiation time, were sequentially optimized to obtain best suited conditions. The 99% degradation of 10 ppm methylene blue was achieved within 60 min of reaction time under pH = 5 and 7, catalyst dose = 10 and 12 mg/100 mL, oxidant = 12 mM and 5 mM for cobalt ferrite and CFA-$CoFe_2O_4$ photocatalysts, respectively. Afterwards, the radical scavenging experiments were conducted to find out the effective radical scavengers ($^{\cdot}OH$, h^+, and e^-) in photocatalytic degradation process. The kinetic study of the process was done by applying 1st order, 2nd order, and BMG models. Statistical assessment of interaction effect among experimental variables was achieved using response surface methodology (RSM).

1. Introduction

Rapid development in the printing, dyeing, and food industries, results heavy discharge of dye wastewater into the environment without their satisfactory treatment. Therefore, the development of effective and economic treatment technologies is the prime need for the wastewater remediation. Conventional treatment technologies include, coagulation, precipitations, ion exchange and biological and electrochemical methods offer certain limitations which resist their application on industrial scale (Chen and Zhu, 2007; Radjenovic and Sedlak, 2015; Rahman et al., 2021; Rubab et al., 2021; Saher et al., 2021). The potential of advanced oxidation processes (AOPs) in developing sustainable technologies for environmental remediations, is being explored from decades. AOPs are aqueous phase oxidation treatments based on the utilization of highly reaction radicles (e.g $^{\cdot}OH$) which predominantly degrade the organic pollutants (Ghanbari et al., 2020, 2021a). The reactive oxygen species (ROS) like $^{\cdot}OH$ degrade the broad range of organic pollutants non-selectively. The different chemical precursors are being used as the source of ROS like hydrogen peroxide, percarbonate, peroxymonosulfate, and peroxydisulfate. These chemical oxidants are

* Corresponding author.
** Corresponding author.
E-mail addresses: Rmzahid@uaf.edu.pk (M. Zahid), asim.jilane@gmail.com (A. Jilani).

https://doi.org/10.1016/j.envres.2021.112280
Received 30 May 2021; Received in revised form 7 September 2021; Accepted 20 October 2021
Available online 28 October 2021

potential candidates for the treatment of industrial wastewater assisted by transition metasl, heat, ultraviolet irradiations, carbon-based catalysts etc (Ghanbari et al., 2021b; Motlagh et al., 2020; Naushad et al., 2019).

Among AOPs, heterogeneous photocatalysts with engineered heterojunctions are emerging material for environmental remediations (Nadeem et al., 2021b; Tabasum et al., 2020, 2021b; Zahid et al., 2019, 2020). The nano ferrites due to their fascinating physicochemical properties and facile synthesis strategies attracted considerable attention of researchers towards their applications in various domains like drug delivery, energy storage devices, wastewater treatment etc (Hassani et al., 2018e). The nanosized magnetite (Fe_3O_4) has been used under heterogeneous sono photo-Fenton process for about 76% removal of BV10 dye within 120 min of reaction time under optimized conditions (Hassani et al., 2018d). The spinel cobalt ferrite ($CoFe_2O_4$) is a cost effective and well known magnetic and electrical semiconductor material. It also owns unique characteristics e.g. (1) easy availability of elements and non-toxicity (2) good catalytic activity due to high surface area (3) narrow band gap (4) easy separation from solution phase due to good magnetic properties (Dou et al., 2020). Furthermore, various studies reported cobalt ferrite when coupled with heterostructures showed high charge transfer ability. For example, $CoFe_2O_4$-rGO hybrids and $CoFe_2O_4$@ZnS core shell nanocomposites were prepared and used for photocatalytic degradation of pollutants from wastewater (Farhadi et al., 2017; He and Lu, 2017). Similarly, Hassani and coworkers (Hassani et al., 2018a) evaluated the sono-catalytic activity of $CoFe_2O_4$-rGO nanocomposites against several organic pollutants and succeeded in achieving more than 90% of pollutants. Other supports like g-C_3N_4 have also been used in combination with other photocatalysts (Eghbali et al., 2019). The combination of g-C_3N_4 with $CoFe_2O_4$ ($CoFe_2O_4$/mpg-C_3N_4, CF/MCN) was developed to improve the properties of pristine cobalt ferrite nanoparticles (Hassani et al., 2018c). The authors reported more than 90% degradation of organic pollutant using mesoporous composite under optimized reaction conditions with PMS as an activator. (Hassani et al., 2018b, 2020). However, high cost (Nadeem et al., 2021a) and instability of photogenerated electrons in pristine metal ferrites limits their application on pilot scale. The prevention in charge recombination can be achieved by compositing these ferrite nanoparticles with other semiconductors having variety of energy band gaps (Nadeem et al., 2021c).

Enhanced performance of ferrite nanomaterials has been achieved by Goyal and coworkers in which they successfully incorporate the Al into the spinel cobalt and nickel ferrite (Goyal et al., 2017). The coal fly ash is a valuable solid industrial waste, but its improper disposal leads towards detrimental effect to soil, environment, and human being (Wang et al., 2020). Wang and coworkers reported an important review on leachability of CFA (Wang et al., 2020). Coal fly ash (CFA), being cheap and rich source of alumina silicate compounds can be used conveniently to enhance the photocatalytic response of $CoFe_2O_4$ nanoparticles. Besides this, various metal oxides present in CFA provides effective sites for heterojunctions. The catalysis is a surface phenomenon, and the photocatalytic activity of spinel ferrite NPs is closely related to their structure (Asma et al., 2019; Moura et al., 2017; Mushtaq et al., 2020; Tabasum et al., 2021a). Insertion of heterojunction (e.g. metals, metal oxides) in cobalt ferrite may improve the cationic distribution for improved photocatalysis as reported previously (Moura et al., 2017).

CFA consists of mostly aluminosilicate compounds. Besides, it also contains several metallic and calcium oxides. Few trace elements (Cr, Ba, Ni, Pb, Sr, and Zn) are also present in FA (Yao et al., 2015), augmented with magnetospheres. Additionally, the water-soluble content (0.2–0.6 wt%) of FAs covers very high concentration of Ca and S, moderate concentration of Ti, Si, P, Na, Mg, K, Fe, Cl and Al and trace amount concentration of Sr, Sn, Ni, Mn, Li and Cs at ppm level, and Zr, Zn, V, Se, Sb, Rb, Pb, Mo, Cu, Cr, Ba and As at ppb level. CFA elements may be considered as network former and network modifiers, which includes Al2O3, SiO2, Fe2O3, P2O5, TiO2 and K2O, Na2O, MgO and CaO respectively. These chemical aspects of CFA suggest them as efficient alternative for metal and metal oxide. The development of cheap catalysts and waste resources into value-added products is being processed nowadays, like CFA into low-cost catalysts. The heterogeneous catalysts synthesis the use of CFA is economically favorable and eco-friendly. The interaction of active catalyst components with some support material is the determining factor for the effectiveness of heterogeneous catalysis. TiO_2, MgO, Al_2O_3 and SiO_2 are widely used metal oxide in catalysis (Wang and Lu, 2007). Thermally stable iron and aluminum oxide are main constituents of CFA. Besides, the high stability of alumino-silicate fractions of CFA in different reactions suggest this material as an efficient support for catalysis (Mushtaq et al., 2019). Wang and colleagues (Wang et al., 2021) modified the raw coal fly ash and used it as an efficient Fenton-like catalyst to treat polymer-flooding wastewater. Effective removal rate (i.e. 70.3%) of polyacrylamide was achieved under optimized reaction conditions. Hence besides other support based $CoFe_2O_4$, the present CFA based $CoFe_2O_4$ nanocomposites are supposed to be the efficient heterogeneous photocatalysts due to the utilization of waste residual material (i.e CFA) as support without any chemical modification.

This study was designed to explore the photocatalytic degradation potential of CFA based cobalt ferrite composite photocatalysts. The composites and cobalt ferrite were synthesized using hydrothermal route and were well characterized using FTIR, XRD, XPS, SEM/EDX and PL analysis. The key influencing reaction parameters were considered for optimization including pH, catalyst dose, oxidant concentration, and reaction time. The kinetic study was conducted using three model including 1st, 2nd, and BMG kinetic models. The radicle scavenging test was performed to better understand the key radicals involved in degradation process. The mutual effect of influencing parameters was studied using a statistical tool "Response Surface Methodology (RSM)". The RSM is a combination of statistical and mathematical techniques developed on multidimensional non-linear model. This model is used for the determination of optimum values of independent variables to produce maximum value of dependent or response variable in wastewater treatment processes (Khataee et al., 2013).

2. Material and methods

2.1. Chemicals

All the materials and reagents used in this research were of analytical grade and used as obtained. The $FeCl_3.6H_2O$ (reagent grade, ≥98%), $CoCl_2.6H_2O$ (ACS reagent, 98%), H_2O_2 (30% w/w), HCl (35% w/w), and NaOH (≥98% BioXtra anhydrous pellets) were bought from Sigma-Aldrich. Ethanol (96%) was obtained from Merck. The sample of CFA was collected from Century paper and Board Mill Lahore. Distilled water was used throughout the experimentation. The methylene blue dye was chosen as representative pollutant.

2.2. Synthesis strategies

2.2.1. Synthesis of $CoFe_2O_4$

Hydrothermal synthesis process was used for cobalt ferrite and its respective CFA composites. In a detailed process, the precursors $CoCl_2.6H_2O$ and $FeCl_3.6H_2O$ were taken into 1:2 mol ratio (0.01 and 0.02 M respectively) and dissolved into 30 mL of distilled water. The mixture was stirred magnetically for 15 min to make it homogenous. Then 3 M NaOH was added dropwise into the above solution until the pH of solution reaches 10. After doing so, the obtained solution was ultrasonicated for 20 min in Digital Ultra Sonicator. The precursors were transferred into Teflon-lined stainless-steel autoclave reactor (250 mL capacity) and place in heating oven at 180 °C for 14 h. After hydrothermal treatment the precipitated were washed for multiple times with the mixture of distilled water and ethanol to remove excess of NaOH. The washed magnetic precipitates of $CoFe_2O_4$ were then air dried in

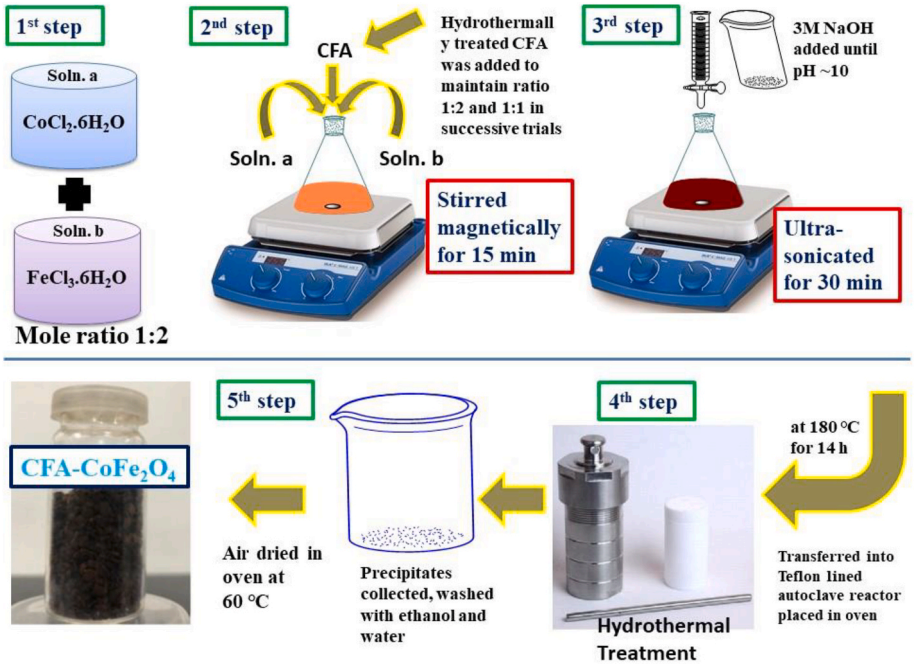

Fig. 1. A schematic illustration for the synthesis of CFA-$CoFe_2O_4$ composites.

oven at 60 °C until dried. The chemical reactions involved during the synthesis of $CuFe_2O_4$ nanoparticles is as below:

$$2CoCl_2.6H_2O + 4NaOH \xrightarrow{-4NaCl,-6H_2O} Co(OH)_2 \rightarrow CoO + H_2O \quad (1)$$

$$2FeCl_3.6H_2O + 6NaOH \xrightarrow{-6NaCl,-6H_2O} 2Fe(OH)_3 \rightarrow Fe_2O_3 + 3H_2O \quad (2)$$

$$CoO + Fe_2O_3 \xrightarrow{Thermal\ treatment} CoFe_2O_4 \downarrow \quad (3)$$

2.2.2. Synthesis of CFA- $CoFe_2O_4$ composites

The CFA chemical composition was determined and categorized as F-type sample (i.e. Al_2O_3+SiO_2+Fe_2O_3>70%) (Nadeem et al., 2021c). The sample of CFA was first thoroughly washed and activated, detailed method is provided in supplementary information, before using in this study. To synthesize composite photocatalysts (CFA-$CoFe_2O_4$), the weighed amount of CFA (for 1:2 and 1:1 wt ratio of $CoFe_2O_4$) was added into the step 2 (section 2.2.1) of the process described for the synthesis of $CoFe_2O_4$ following rest of the synthesis protocol same. The CFA composite owed large specific surface area with micro-pore, large enough to house the dye molecules. The flow chart for synthesis process is described in Fig. 1.

2.3. Characterizations

The as synthesized $CoFe_2O_4$ NPs and composite photocatalysts (CFA-$CoFe_2O_4$(1:2) and CFA-$CoFe_2O_4$(1:2)) were well characterized with different analytical techniques. The CFA chemical composition was determined using XRF analysis and reported previously (Nadeem et al., 2021c). The phase analysis of synthesized catalysts was done using X-ray diffractometer (XRD, Rigaku) with source of Cu-Kα radiation (λ = 0.154056 nm) at an operating current of 40 mA and voltage of 45 kV. The identification of surface functional groups of catalysts was carried out using Fourier-transform infrared (FTIR) spectroscopy (PerkinElmer spectrum 100 spectrometer). The elemental analysis and surface chemical composition was determined using X-ray photoelectron spectroscopy (XPS; XPS; Escalab 250 XPS system, Thermo Fisher Scientific UK). The surface morphology was determined using Scanning electron microscope (SEM JSM-7000 F, ACCEL VOLT 10.0) and near surface elemental analysis were done by energy dispersive spectroscopy (EDS) attached with SEM. Shimadzu RF-5301 was used to acquire the charge recombination ratio prepared composites. To check the percentage degradation of dyes the UV–Visible spectrophotometer (CECIL CE 7200).

The surface properties of a photocatalysts plays vital role in the adsorption of pollutants molecules. The effective adsorption assures enhanced photocatalysis of adsorbate. Therefore, the surface charge of the photocatalysts was determined using pH drift method. The detailed process is described in the supplementary document of this article.

2.4. Photocatalytic degradation experiments

Photocatalytic degradation was carried out under UV 254 nm light source. The detailed description about the light source and methodology to treat the dye solution is provided in the supplementary information document.

2.5. Kinetic study

The Fenton processes are complicated and multistep processes and therefore their kinetic study is important for the complete understanding of reaction mechanism. The kinetics of dye degradation is usually described by different kinetic models. For present research three different kinetic model namely 1st order reaction kinetic model Eq. (4), 2nd order reaction kinetic model Eq. (5), and Behnajady-Modirashahla-Ghanbery kinetic models Eq. (6) were selected for MB degradation reaction mechanism study. The best suited model was proposed for the reaction mechanism of dye degradation for each catalyst.

$$1^{st}\ \text{order kinetics}\ ln\frac{C_o}{C_t} = k_1.t \quad (4)$$

$$2^{nd}\ \text{order kinetics}\ \frac{1}{C_t} - \frac{1}{C_o} = k_2.t \quad (5)$$

$$\text{Behnajady} - \text{Modirashahla} - \text{Ghanbery kinetics}\ t \div \left(1 - \frac{C_t}{C_o}\right) = m + b.t \quad (6)$$

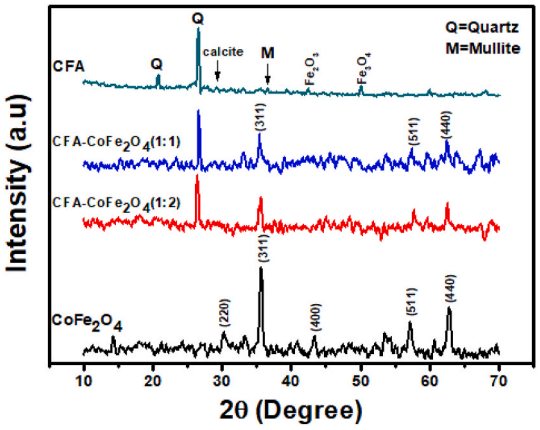

Fig. 2. XRD pattern of $CoFe_2O_4$ and CFA-$CoFe_2O_4$ composites.

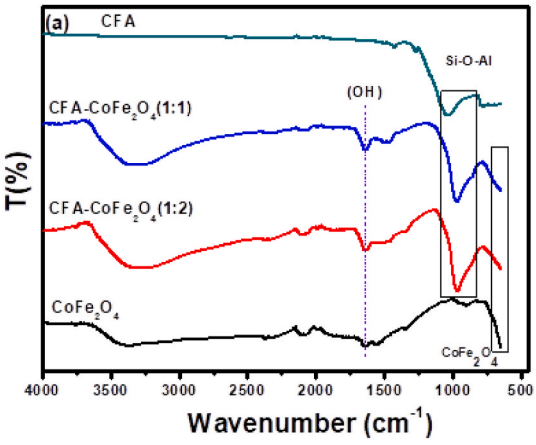

Fig. 3. FTIR of $CoFe_2O_4$ and CFA-$CoFe_2O_4$ composites.

2.6. Response surface methodology

Response Surface Methodology (RSM) is a statistical tool to optimize the process like photocatalytic oxidative degradation of organic pollutants. It is a mixture of mathematical and statistical techniques which offer improved way of interactions among controllable experimental factors with reliable results. This methodology helps in the prediction of two or above two variables at once by executing statistical experimental design. The efficient evaluation of model and cumulative response can be predicted using RSM.

In this research, the central composite design (CCD)-under RSM-was used. The advantage of CCD is the enough information provided by the design at relatively less experimental runs. In this way providing overall cost-effectiveness with experiments. The goodness of fit was obtained, running 2^3 factorial CCD with three variables (dye dose, oxidant dose, and catalyst dose) by running 20 experiments with 8 factorial, 6 axial, and 6 central replicates using following formula;

$$N = 2^n + 2n + n_c = 2^3 + 2 \times 3 + 6 = 20$$

where.

N = the total number of experiments to be performed
n = the number of factors to be studied

The independent variables were dye dose (A), oxidant dose (B), and catalyst dose (C) whereas percentage degradation of MB was the response variable at constant pH, reaction time, and light source (UV).

The five levels for every independent variable were $X_i = -1.68, -1$, 0, 1, and 1.68. Least square test using second order model was selected for the interpretation of the correlation between three independent variables (dye dose, oxidant dose, and catalyst dose) while response variable was percentage degradations. The equation for second order model is as below (Eq (7));

$$Y = \beta_o + \sum_{i=1}^{k} \beta_i X_i + \sum_{i=1}^{k} \beta_{ii} X^2{}_i + \sum_{i=1}^{k} \sum_{i \neq j=1}^{k} \beta_{ij} X_i X_j + \varepsilon \quad (7)$$

Here Y is the response variable (i.e., % degradation), β_o is the numerical coefficient and β_i is the coefficient of linear effects, $\beta_{ii}$is for quadratic effects, and $\beta_{ij}$is the coefficients related with interaction effects. k is the numeral of independent variables and Epsilon (ε) is the random error. The pure error estimation in CCD is done performing three replicate experiments at central point. Incomprehensible variability on response was abated by performing random experiments. Response surfaces and contour plots were produced for MB dye degradation using CFA-$CoFe_2O_4$(1:1) in the given range of condition using "Design Expert 7.0.0" software. The suitability and validity of models was determined as per their significance by calculating F-values statistically at probability factor (p) of 0.05 (F-test) and goodness of fit (R^2) by analysis of variance (ANOVA).

3. Results and discussion

3.1. Structural, functional, compositional, and optical analysis

The XRD pattern of CFA, $CoFe_2O_4$ and it composites with CFA (CFA-$CoFe_2O_4$ (1:2), CFA-$CoFe_2O_4$ (1:1)) is shown in Fig. 2. The XRD of CFA displays the characteristic peaks of quartz (Q), mullite (M), calcite ($CaCO_3$), hematite (Fe_2O_3), magnetite (Fe_3O_4). The crystalline planes in the diffraction pattern of $CoFe_2O_4$ are labelled as (220), (311), (400), (511), and (440) as described previously (Gastelo et al., 2019) (JCPDS: Card # 22–1086) which are the representation of spinel structure of $CoFe_2O_4$. The composites of $CoFe_2O_4$ with CFA showed characteristics peaks corresponding to both CFA and $CoFe_2O_4$ which reflect the successful synthesis of CFA-$CoFe_2O_4$ nanocomposites (Fig. 2).

The crystal size, d_{XRD} of prepared materials were calculated using the Debye-Scherrer equation

$$D = \frac{K\lambda}{\beta cos\theta} \quad (8)$$

Here, K is the Scherrer constant (value 0.94), λ is the X-ray wavelength (0.154 nm), β is the FWHM (full width at half maximum) of photocatalysts, D is calculated crystalline size and θ is the diffraction angle. The average crystallite size of $CoFe_2O_4$, CFA-$CoFe_2O_4$ (1:2), CFA-$CoFe_2O_4$ (1:1), and CFA was estimated to be 15.4 nm, 22.8 nm, 23.5 nm, and 29.4 nm respective. The little enhancement in crystalline size of CFA- $CoFe_2O_4$ as compared to pristine $CoFe_2O_4$ is attributed to the incorporation of CFA particles (Nadeem et al., 2021c) whereas, reduction in crystalline sized of composite as compared to pristine CFA is due to the insertion of smaller dimensional $CoFe_2O_4$ nanoparticles (Nadeem et al., 2021a).

The surface functional groups of CFA, $CoFe_2O_4$, and its composites with CFA were characterized using FTIR spectroscopy and resultant spectra's are presented in Fig. 3. The FTIR of CFA exhibits asymmetric stretching vibrations at 1041 cm^{-1} accredited to Si–O–Al that shifted at lower values of 965 cm^{-1} in composite photocatalysts. The high intense peak at ~580 cm^{-1} is attributed to the Fe–O stretching vibration in $CoFe_2O_4$ and CFA-$CoFe_2O_4$ composite photocatalysts (Nadeem et al., 2020; Zhao et al., 2005). The existence of an absorption band corresponding to the stretching vibration of the Fe–O bond confirms the successful loading of $CoFe_2O_4$ on CFA. The band at ~3390 cm^{-1} and peaks at1645 cm^{-1} were attributed to the bending and stretching vibrations of OH groups and surface adsorbed H_2O molecules. In CFA composites, the peaks around 1400-1500 cm^{-1} is due to the carbonated

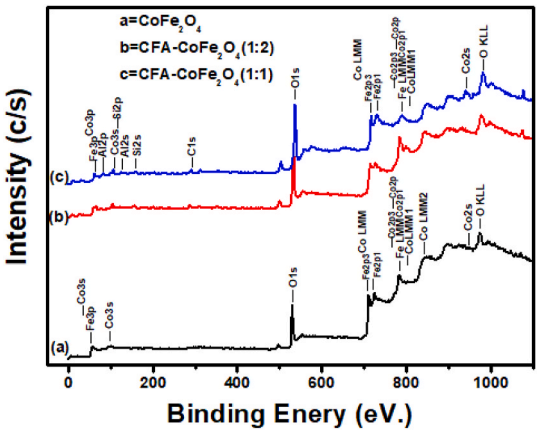

Fig. 4. XPS survey scans of $CoFe_2O_4$ and its CFA composites.

Table 1
Detected composition of $CoFe_2O_4$ and its composites with coal fly ash through XPS survey spectra.

Sample detail	Composition (Atomic %)					
	O1s	Co2p3	Fe2p3	C1s	Si2p	Al2p
$CoFe_2O_4$	71.8	16.8	11.4	–	–	–
CFA-$CoFe_2O_4$ (1:1)	62.6	12.7	3.7	9.8	8.0	3.0
CFA-$CoFe_2O_4$ (1:2)	57.6	14.3	9.4	8.3	10.4	–

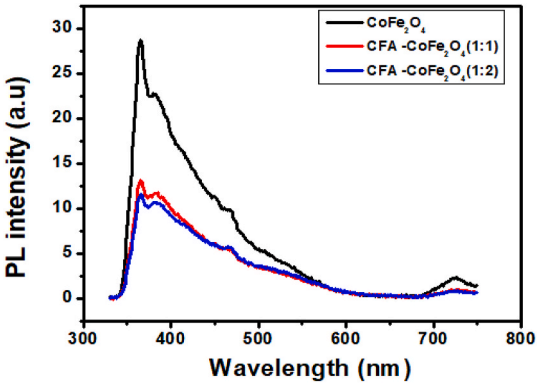

Fig. 5. PL spectra of $CoFe_2O_4$ and CFA-$CoFe_2O_4$ composites.

species ($CaCO_3$) which is originated due to the reaction of calcium hydroxide with atmospheric CO_2 (Clara and Sugirtha, 2016; Mozgawa et al., 2014).

The catalytic activity of nanocomposites catalysts may be effected by its elemental composition (Jilani et al., 2020) therefore X-ray photoelectron spectroscopy was employed to reveal the composition of cobalt ferrite and its composites. The surface compositional analysis are presented in Fig. 4. The main composition of cobalt ferrite consisted of O1s, Co2p3 and Fe2p3 having around 71.8%, 16.8 and 11.4% respectively. This also affirms the accuracy of synthesis procedure. In case of CFA--$CoFe_2O_4$ (1:1 and 1:2) additional peak of C1s was noticed which was attributed to the presence of coal fly ash in the composites. However, some additional peak of Al2p and Si2p was also observed which is the constituent of coal fly ash. Further, the atomic percentage of C1s was changed which was expected due to the change in ratio *i.e.* 1:1 and 1:2. The atomic percentage of all the elements for the prepared samples is shown in Table 1.

Fig. 5 shows the photoluminescence spectra of cobalt ferrite and its CFA composites recorded at the excitation wavelength of 330 nm. Emission of PL means the recombination of electron hole pair. Higher the PL emission higher is the recombination of charge carries. This poor charge separation retards the photocatalysis process (Choi et al., 2015). The PL of cobalt ferrite was recorded quite different from that of its CFA composites with the reduction in PL intensity in the order of $CoFe_2O_4$>CFA-$CoFe_2O_4$(1:2)>CFA-$CoFe_2O_4$(1:1). The bandgap edge shifts to the longer wavelength with the insertion of CFA into CoF_2O_4. This shifting of band edge to longer wavelength attributed to the rapid charge carries movement with sluggish recombination ratio, which is preferable for the enhanced photocatalytic activity of the subjected material. Therefore, the PL finding order $CoFe_2O_4$>CFA-$CoFe_2O_4$(1:2)> CFA-$CoFe_2O_4$(1:1) is also consistent with our photocatalytic results.

The surface morphological survey of the catalysts and composite photocatalysts was examined using SEM imaging (Fig. 6). The SEM revealed cubic morphology of $CoFe_2O_4$ particles with regular structure. The composites provide irregular morphology. The improved roughness and irregular surfaces in the composite photocatalysts are responsible for the well performance of the composites. The improved surface roughness results improved fractional dimensions which provide high surface interaction compared to even surfaces (Venkatakrishnan and Kuppa, 2018).

The EDS of cobalt ferrite and its CFA composites provide clear indication for elemental distribution. The existence of Al and Si (important constituents of CFA) along with other elements is evident in composite photocatalysts.

The results of pHpzc are presented in Fig. 7 and showed that pHpzc increases with the insertion of CFA into copper ferrite. The reason of this could be explained based on the negative surface groups present on CFA in aqueous solutions.

3.2. Photocatalytic study

3.2.1. Effect of pH

The effect of pH on percentage degradation of MB was checked and the results are presented in Fig. 8(a). The graphs clearly demonstrate that pH plays important role on the degradation of MB dye by all the catalysts. The pH of initial dye solution is the driving factor in adsorption process which influence the functional groups located on the surface of catalyst and degree of ionization of pollutants. The best degradation potential of CFA-$CoFe_2O_4$ nanocomposites was observed at pH 7. The effective degradation at pH 7 is attributed to the negative surface charge groups of CFA at pH 7. Further, the results of pH effect can be corelated with the results of pH_{pzc} (Fig. 7). The result makes good correlation agreement as the CFA-$CuFe_2O_4$ nanocomposites exhibits best performance at pH > pH_{pzc} of the material. At higher value i.e., pH > pH_{pzc} the surface of the composites becomes negatively charges which attract the adsorption of cationic MB therefore betterer adsorption with enhanced photocatalytic degradation was achieved.

In the case of cobalt ferrites, the possible reason for lower degradation under alkaline condition of dye solution, may be attributed to the reaction between Fe^{2+} ions and OH radicals Eq. (13). The reaction is followed by the generation of $Fe(OH)_{2\ surface}$(a yellowish-brown sludge) Eq. (14). The generation of sludge at higher pH cover the surface of catalysts and reduces the interaction of targeted pollutant molecule with the surface of catalyst by blocking the active sites.

The change in behavior under alkaline condition was observed with CFA composites. In alkaline conditions the new active sites ($\equiv SiO^-$)and ($\equiv AlO^-$)develop on the surface of FA which promote the adsorption of cationic MB dye Eqs. (9) and (10).

$$2(\equiv SiO^-) + MB^+ \rightarrow (\equiv Si-O)_2MB \quad (9)$$

$$2(\equiv AlO^-) + MB^+ \rightarrow (\equiv Al-O)_2MB \quad (10)$$

3.2.2. Effect of catalyst dose

Determining the amount of catalyst dose plays crucial role for the economic assessment and efficiency of the material. Therefore, a range

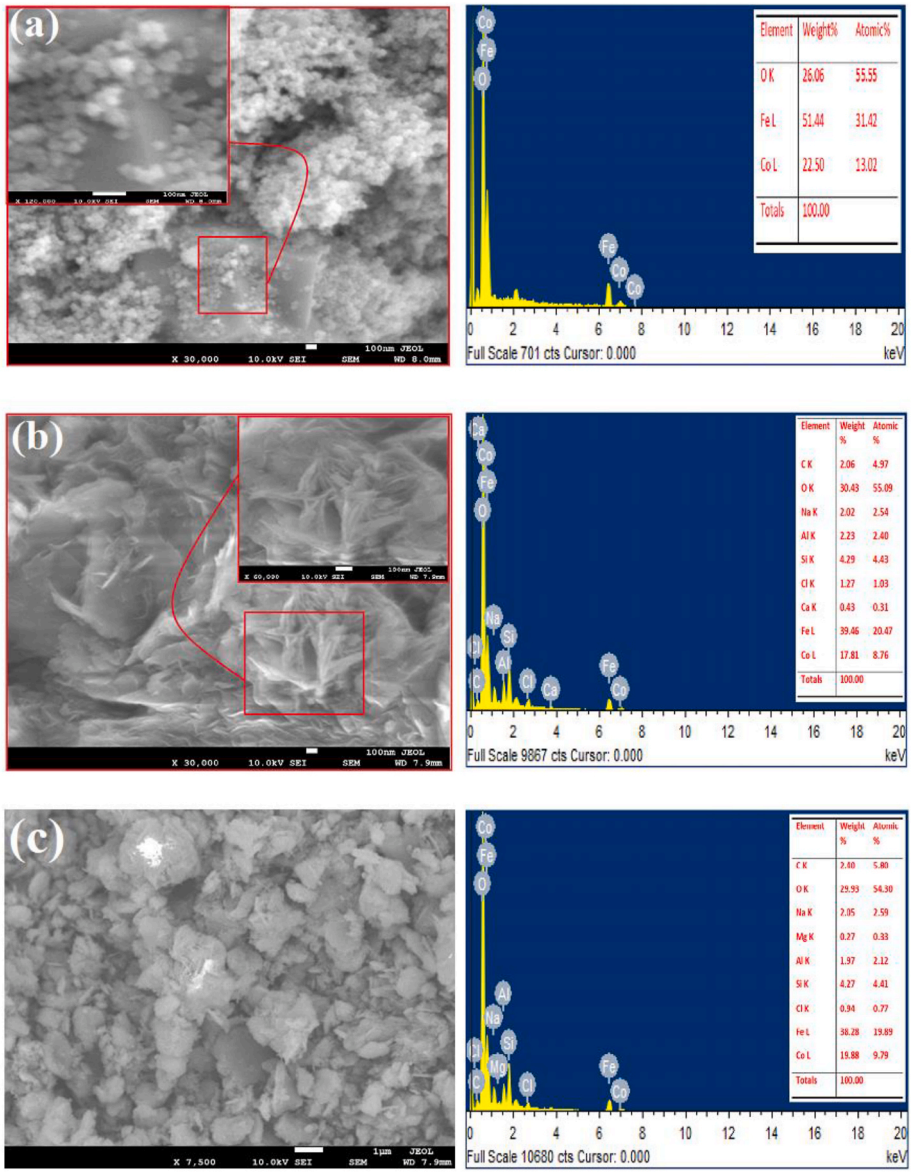

Fig. 6. SEM/EDS analysis of a) $CoFe_2O_4$ b) CFA-$CoFe_2O_4$ (1:2), and c) CFA-$CoFe_2O_4$ (1:1).

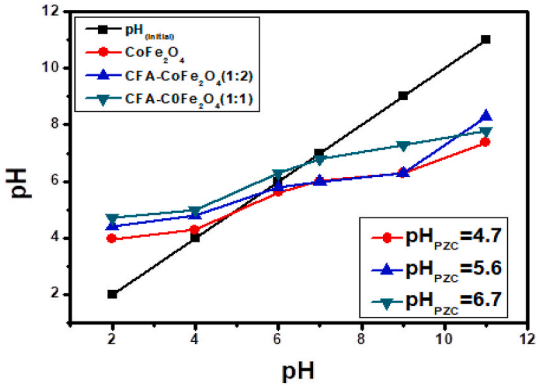

Fig. 7. pH_{pzc} for $CoFe_2O_4$ and its CFA composites.

of catalysts dose (20–260 mg/L) was chosen for selecting the optimized concentration of catalysts for current study. The results obtained are presented in Fig. 8(b).

The results present the effective increase in the photocatalytic degradation of MB dye with the increase in the catalyst dose up to certain limit. For example, as the catalyst dose increases from 2 to 12 mg/100 mL the value of percentage degradation increases from ~50 to 87% and 53–99% using CFA-$CoFe_2O_4$(1:2) and CFA-$CoFe_2O_4$(1:1), respectively (see Fig. 8(b)). This potential increase in the degradation efficiency of CFA composite photocatalysts is attributed to the increase in the adsorption capacity of composites (high active adsorption sites) which improves the photocatalytic degradation of adsorbed MB. Additionally, it promote the generation of hydroxyl radicals in Fenton-like reaction see Eq (11)(12), and e^-/h^+ pair (Huang et al., 2008; Shaban et al., 2017, 2018a) which accelerate the photo-Fenton reaction (Shaban et al., 2018b).

$$Fe^{2+} + H_2O_2 \rightarrow Fe^{3+} + OH^- + OH^{\cdot} \quad (11)$$

$$Fe^{3+} + H_2O_2 \rightarrow Fe^{2+} + HO_2^{\cdot} + H^+ \quad (12)$$

On the other hand, the degradation potential of pristine cobalt ferrite also increases from 31% to 62% when catalyst dose increases from 2 mg/100 mL to 10 mg/100 mL. Interestingly, the degradation achieved using cobalt ferrite dose not exceeds from ~65% even when catalyst dose

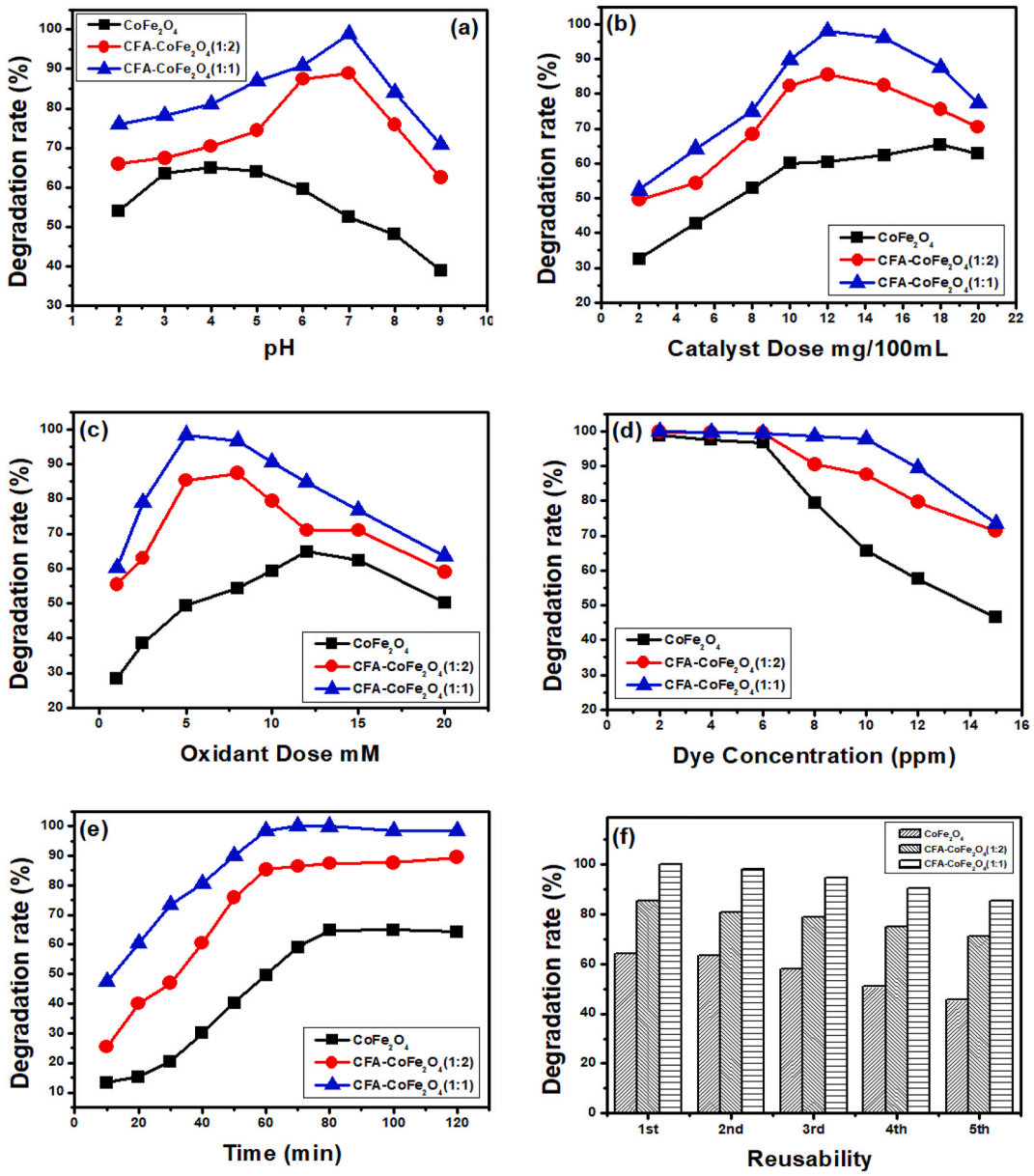

Fig. 8. Efect of influencing reaction parameters on photocatalytic degradation of MB (a) pH, (b) catalyst dose, (c) oxidant dose, (d) dye concentration, (e) irradiationo time, and (f) reusability of photocatalysts under experimental conditions of pH = 4 and 7, cat. Dose = 18 and 12 mg/100 mL, H_2O_2 = 12 and 8 mM, T = 80 and 60 min, using CoF and CFA-based CoF respectively and MB = 10 ppm under UV 254 nm.

increased further. This saturation towards degradation efficiency may be due to the limitations offered by metal ferrites when used in pristine form (Zahid et al., 2019). However, the addition of CFA into $CoFe_2O_4$ improves the efficiency remarkably. This better performance of composite photocatalysts is due to the enhanced adsorption efficiency which is due to increase in surface roughness of composites (as the SEM imaging indicates Fig. 6). Increasing the roughness implies the increase in surface defects and possible increase in high energy active sites. These high energy active sites are responsible for the promotion of the adsorption capacity of CFA based cobalt ferrites followed by rapid photocatalytic degradation of adsorbed pollutants.

Additionally, the lower values of %degradation was observed by increasing the catalysts dose above optimized values. This behavior is due to the disturbance of balance between catalyst to dye ratio, the reactive oxygen species (OH) is scavenged by the excess Fe^{2+} ions as presented in Eq (13). Further, the Fe^{3+} will react with HO^-produced in Eq (13) to generate sludge $(Fe(OH)_{2\ surface}$ Eq. (14).

$$\dot{O}H + Fe^{2+}_{surface} \rightarrow Fe^{3+}_{surface} + HO^- \quad (13)$$

$$2HO^- + Fe^{3+}_{surface} \rightarrow Fe(OH)_{2\ surface} \quad (14)$$

3.2.3. *Effect of oxidant dose*

Addition of hydrogen peroxide results boost in photocatalytic degradation of MB dye. The hydrogen peroxide is responsible for the generation of hydroxyl radicles which results in surface activation of catalysts. This surface activation promote the affinity for dye molecules to be adsorbed (Visa et al., 2015; Zuorro and Lavecchia, 2014). All the experiments were conducted under optimized conditions of contact time, solution pH, substrate concentration, and initial dye concentration.

The results obtained for the optimization of H_2O_2 dose are presented in Fig. 8(c). Effective increase in response variable was observed with the increase in the oxidant dose. This increase is due to the hydroxyl

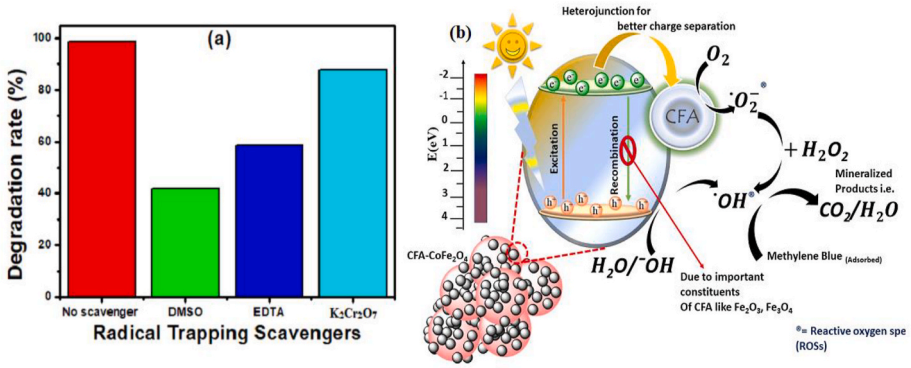

Fig. 9. (a) Radical trapping experiment and (b) Proposed photocatalytic degrdadation mechanisim of MB using CFA-$CoFe_2O_4$(1:1).

radicals generated during reactions presented in eq. (18)(19). The detailed mechanism for oxidative photocatalytic degradation of MB has been presented in Fig. 8(b) it was observed that the further increase in oxidant dose (i.e. above the optimized values) pose negative impact of dye degradation (Enesca et al., 2014; Visa et al., 2015). It has been reported that, the overdosage of hydrogen peroxide results in the generation of hydrogen peroxide radical ($HO_2^{\cdot}$) which are the less reactive radical than $HO^{\cdot}$ radicals and it also act as $HO^{\cdot}$ scavenger according to eq. (15)(16). Therefore, results in deactivation of effective OH radicles present in reaction system.

$$H_2O_2 + \dot{O}H \rightarrow H_2O + HO_2^{\cdot} \quad (15)$$

$$HO_2^{\cdot} + \dot{O}H \rightarrow H_2O + O_2 \quad (16)$$

The h^+ also plays positive role in degradation as the results of scavenging experiment indicates (Fig. 8(a)). The overdosage of H_2O_2 can react with holes (from valance band) on catalyst surface results in oxygen formation and $^{\cdot}OH$ inhibition. This promotes the overall reduction in degradation efficiency eq. (17).

$$H_2O_2 + 2h_{VB}^+ \rightarrow O_2 + 2H^+ \quad (17)$$

Here is the detail which presents the potential role of hydrogen peroxide in generation of effective radicles. The role of hydrogen per oxide in radicle generation followed well known mechanism in dye degradation. The high concentration of $HO^{\cdot}$ produced in eq. (18) also act as electron acceptor which promote charge separation (eq. (19)) (Chu et al., 2007):

$$H_2O_2 + O_2^{\cdot-} \rightarrow HO^- + \dot{O}H + O_2 \quad (18)$$

$$H_2O_2 + e_{(CB)}^- \rightarrow HO^- + \dot{O}H \quad (19)$$

Besides, the low or unavailability of hydrogen peroxide in the locality of the photocatalyst, the e^-/h^+ recombination increases, and the absorbed energy is dissipated as heat. However, the excess availability of hydrogen peroxide supports the decomposition of hydrogen peroxide into water and oxygen up to certain limit. Therefore, the optimum dose of hydrogen peroxide is crucial in achieving best photocatalytic efficiency (Chu et al., 2007).

3.2.4. Effect of dye concentration

The effect of different dye concentration in simulated wastewater was studied. The different concentration solutions in ppm level were selected for photocatalytic oxidative degradation study by keeping rest of the parameters (i.e. pH, catalyst does, oxidant dose, irradiation time) constant. The 2–15 ppm solutions of MB were used for photocatalytic degradation. The results obtained are presented in Fig. 8(d).

The results reflect that, the 10 ppm solution of MB was effectively degraded within 60 min of reaction time using all catalysts. The complete degradation of dyes below 10 ppm concentration could justify by the fact that excessive catalytic active sites were available for limited targeted dye molecules. However, as the concentration reached their optimum values the balance between active sites and dye molecules was achieved above which increasing the dye concentration showed no effective response. The lower degradation with increasing the dye load in due to the disturbance caused by the unavailability of active sites for degradation.

Further, the lower degradation at higher dye concentration is due to the affected transparency of solution. Further, increasing the dye concentration results reduction in oxidant to dye ration which pose negative impact on photocatalysis (Nidheesh et al., 2013).

3.2.5. Effect of irradiation time

Optimization of reaction time is crucial for effective implementation of any chemical process. Therefore, the effect of different time intervals (10–120 min) was observed **(Fig. 8(e))** for MB degradation. After starting the photocatalytic reaction under the aliquots were withdrawn from the reaction mixture with subsequent intervals and reduction in dye concentration was checked using a UV–Visible spectrophotometer. At the start of reaction, the considerable enhancement in degradation was observed wich slowdown over time. The maximum photocatalytic degradation of MB using $CoFe_2O_4$ and CFA-$CoFe_2O_4$ composites was reached within 60 min of reaction times.

3.2.6. Stability/reusability analysis of catalysts

The advantage of heterogeneous photocatalysts is their facile separation from reaction mixture and multiple reusability potential. Therefore, stability analysis of catalysts was checked in term of their reusability. The results obtained for five successive reusability runs are presented in Fig. 8(f). The results showed considerable efficiency of photocatalysts even used after multiple times. To effectively predict the better efficiency performance of catalysts, AAS (atomic absorption spectroscopic) analysis was conducted.

The Fe element is the main component of active sites of prepared catalysts (Hu et al., 2018; Leifeld et al., 2018; Messele et al., 2018; Xu et al., 2018). Several other metallic elements like Mn, Zn, Pb, Cu etc also exhibited enhanced catalytic potential and CFA contains multiple metallic elements such as Fe, Mn, Zn, Cu, Pb and others (Wang et al., 2018, 2019). So, the catalytic performance of all the proposed composites (CFA based metal ferrite) is promoted by the co-catalysis of metallic elements present on the surface of CFA.

The Fe leaching test results showed 0.99, 0.74, and 0.49 ppm Fe leached after 5th reusability run using $CoFe_2O_4$, CFA-$CoFe_2O_4$(1:2), and CFA-$CoFe_2O_4$(1:1) respectively. However, the current work suggests that the AAS analysis confirm the low leaching of Fe into treated solution even after 5 reusability runs. Further, the stability comparison between pristine cobalt ferrite and CFA-$CoFe_2O_4$ composites revealed that the immobilized cobalt ferrites over CFA show minimum leaching. The immobilization not only improves the photocatalytic performance but

Table 2
Values of co-efficient of correlation and rate constant of MB degradation using cobalt ferrites and their CFA composites.

Catalyst	1st order		2nd order		BMG model		
	R^2	K_1 (min^{-1})	R^2	K_2 (L $\mu mol^{-1} min^{-1}$)	R^2	m (min^{-1})	B
$CoFe_2O_4$	0.89	0.009	0.89	0.0002	0.96	61.48	0.91
CFA-$CoFe_2O_4$(1:2)	0.95	0.244	0.92	0.0009	0.95	31.67	0.79
CFA-$CoFe_2O_4$(1:1)	0.94	0.977	0.72	0.4044	0.99	13.29	0.87

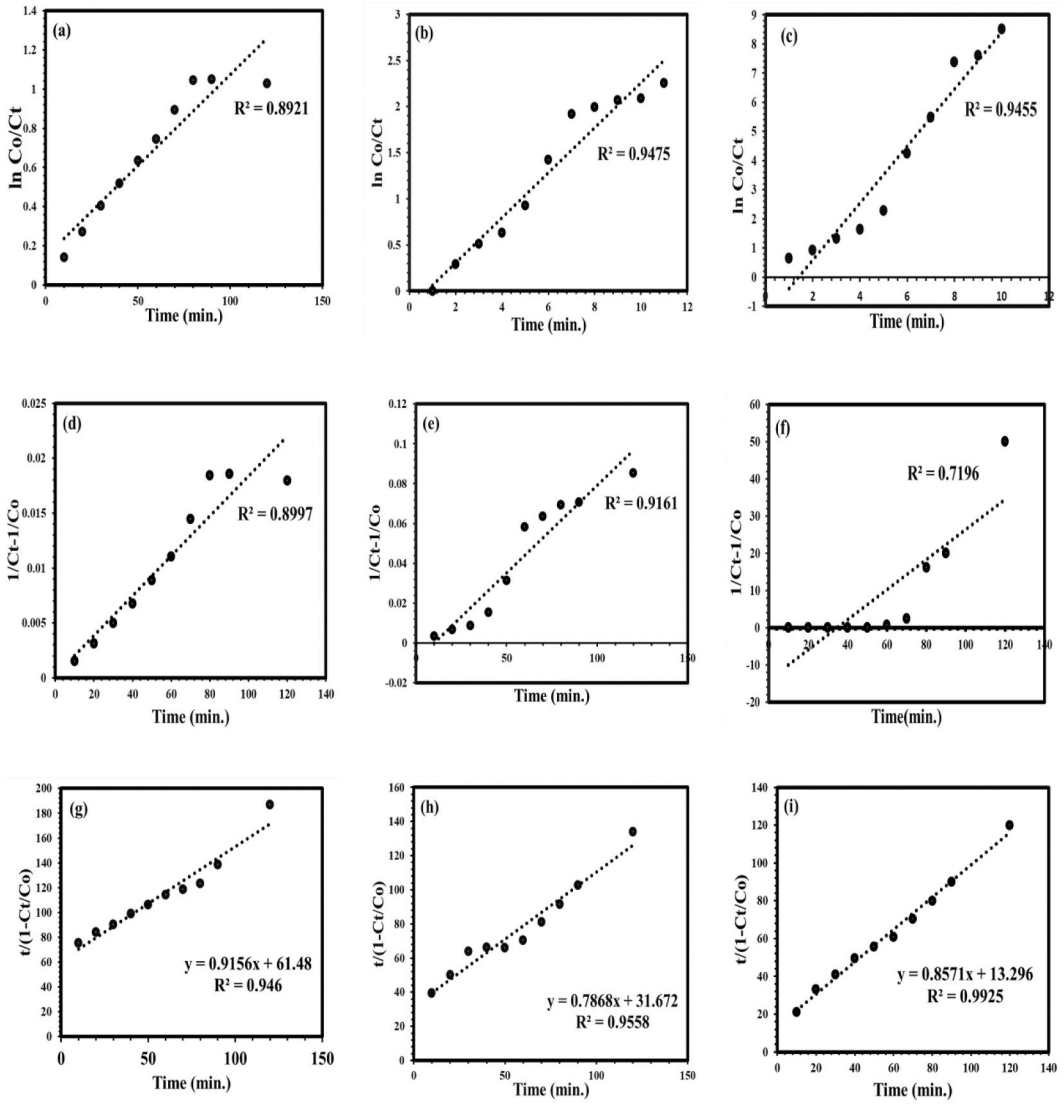

Fig. 10. Kinetic models for the degradation of MB (a,b,c) 1st order, (d,e,f) 2nd order, and (g,h,i) BMG using (a,d,g)$CoFe_2O_4$, (b,e,h) CFA-$CoFe_2O_4$(1:2), and (c,f,i) CFA-$CoFe_2O_4$(1:1).

also resist the leaching of Fe into water. Therefore, the CFA based copper ferrite composites were found to be the stable photocatalysts for the treatment of wastewater even after 5 reusability runs. Besides, the magnetic character of composite helped in achieving fast separation of photocatalyst from the reaction material **(Fig.S-2).**

3.2.7. Radical scavenging experiment and proposed degradation mechanism using CFA-$CoFe_2O_4$(1:1)

The radicals play important role in photocatalytic degradation process, therefore, the effective radicals were determined. In this respect, radical scavenging experiment was performed to find out the potential radicals (holes, and electron etc.) involved in photodegradation of dye (Shao et al., 2017, 2018, 2020; Sharma et al., 2018). The 10 mM solutions of DMSO (dimethyl sulfoxide) to scavenge OH radicals, EDTA (ethylene-diamine-tetra-acetate) to scavenge holes, and $K_2Cr_2O_7$ (potassium dichromate) to scavenge electrons were used (Nadeem et al., 2021a). The UV accelerated experiments were conducted under optimized conditions of other parameters. The results are presented in Fig. 9 (a). The results showed that DMSO was the primary radical scavenger in photocatalysis process. The addition of DMSO results decrease in the degradation values from 99% to 41% using CFA-$CoFe_2O_4$(1:1) composite photocatalyst. Similarly, the results showed effective contribution of holes as the EDTA reduces the degradation of MB from 99% to 66%. Whereas, the addition of $K_2Cr_2O_7$ found no considerable decrease in response variable. This confirm the very small contribution of electrons in photodegradation.

Considering the effectiveness of hydroxyl radicals and holes the proposed degradation mechanism is presented in Fig. 9(b). It can be described as: In general process, an electron hole pair is produced under light source with excitation energy ≥ the energy bandgap of the material. The ferrite nanoparticles have the disadvantage of rapid charge recombination as can be seen in the PL spectra of CoF_2O_4 **(Fig. 5)** showing high emission intensity. While compositing CoF_2O_4 with CFA provides considerable reduction in emission intensity which is a strong evidence of efficient creation of trapping sites (heterojunction) for reactive species. The important constituent of CFA that take part in prevention in charge recombination may include Fe_2O_3, Fe_3O_4, etc (Nadeem et al., 2021c). The holes (h^+) take part in ȮH radical formation. These strong oxidizing species are efficient to degrade the adsorbed dye molecules (near the surface of the photocatalyst) into smaller fragments, which can be further adsorbed on the substrate active sites where they may degrade up to mineralized products eq. (20).

$$\dot{O}H + Dye \rightarrow CO_2 + H_2O + mineralization\ products \quad (20)$$

3.3. Kinetic study

In proposed project, 1st order, 2nd order, and BMG reaction kinetics were employed to investigate the degradation kinetics of MB dyes by Fenton Oxidation process (FOP). The individual expressions are presented in Table 2. The K_1 and K_2 are the kinetic rate constants for 1st order and 2nd order reactions, respectively. The regression analysis for 1st order and 2nd order reactions was conducted and presented in Table 2 and Fig. 10.

The results demonstrate that, the 1st order and 2nd order regression co-efficient and rate constants increase with the insertion of CFA into cobalt ferrites. Considering the values for the 2nd order kinetic model similar trend was observed among the native metal ferrites and their CFA composites. However, the comparison of rate constants for the 1st order and 2nd order kinetic models provides clear evidence that the 1st order kinetic model is more suitable for FOP. On the other hand, Guedes and coworkers (Guedes et al., 2003) proposed that FOP is a 2nd order reaction. Anyhow, the information about kinetic study for the degradation of organic pollutants by FOP was limited before the development of BMG kinetic model. Which was specifically designed for the oxidative degradation of organic pollutants following FOP.

Considering the correlation coefficient values of the reaction kinetic containing CFA-M-Fe_2O_4(1:1), the BMG kinetic model was best fitted to the experimental data as the highest R^2 values were observed as compared to the 1st order and 2nd order kinetic model.

The degradation process using heterogeneous photo-Fenton process proceeds by two steps. 1st: the reaction between Fe^{2+} and H_2O_2 Eq. (11), 2nd: the slow stage attributed to the accumulation of ferric (Fe^{3+}) ions and low Fe^{2+} recovery by H_2O_2 (Barreto et al., 2016; Malik and Saha, 2003; Santana and Aguiar, 2015). Chu and coworkers reported the similar performance for 2,4-dichlorophenoxyacetic acid degradation by Fe^{2+}/H_2O_2 (Chu et al., 2004). The reaction goes with very fast stage followed by slower one, therefore, not 1st nor 2nd order could be modeled perfectly. Hence, BMG kinetic model was chosen to present the kinetic of Fe^{2+}/H_2O_2 system. The highest goodness of fit to the model was achieved using CFA-$CuFe_2O_4$(1:1) composite **(Fig. 10).** This suggest that CFA composite photocatalyst exhibit improved FOP.

3.4. Response surface methodology for optimizing parameters using CFA-$CuFe_2O_4$(1:1)

RSM was opted for parameter optimization and identification of interaction among parameters. Three independent variables (i.e. composite dose, H_2O_2 dose, and dye dose) were chosen and mutual interaction was studied using central composite design (CCD) (Sharma and Satyanarayana, 2006). The Design Expert 7.0.0 software was used for this purpose and optimization of parameters was done to understand the possible combinational interactions and impact of individual parameter on response variable. The independent variables were set "within range" and "maximum value" for response variable (% degradation) was obtained after experimentation. The CCD proposed 20 experimental trial which were accomplished to produce response surfaces (3D and contour plots). The ANOVA results delivers statistical assessment about the significant factors with possible interactions. The ANOVA results and co-efficient of distribution values along with R^2 values for the degradation of MB using CFA-$CoFe_2O_4$(1:1) are presented in Table 3.

Table 3
ANOVA results of quadratic model for degradation of MB using CFA-$CoFe_2O_4$ (1:1).

Source	Sum of Squares	df	Mean Square	F-value	p-value Prob > F	Remarks
Model	9728.74	9	1080.97	90.82	<0.0001	Significant
A- dye conc.	4.27	1	4.27	0.36	0.5625	
B-catalyst dose	402.45	1	402.45	33.81	0.0002	
C-oxidant dose	1279.34	1	1279.34	107.48	<0.0001	
AB	0.13	1	0.13	0.011	0.9204	
AC	78.133	1	78.13	6.56	0.0283	
BC	78.13	1	78.13	6.56	0.0283	
A^2	2340.86	1	2340.86	196.67	<0.0001	
B^2	3261.15	1	3261.15	273.98	<0.0001	
C^2	3819.74	1	3819.74	320.91	<0.0001	
Residual	119.03	10	11.90			
Lack of Fit	94.37	5	18.87	3.83	0.0835	Not significant
Pure Error	24.66	5	4.93			
Cor Total	9847.77	19				
Std. Dev.	3.45		R-squared		0.9879	
Mean	66.75		Adj. R-squared		0.9770	
C.V.	5.17		Pred. R-squared		0.9226	
Press	762.02		Adeq. Precision		25.548	

3.4.1. Optimization and interaction effects of influencing parameters

The combined effect of composite and H_2O_2 dose is shown in Fig. 11 (a). The range of operating parameters for composite and oxidant dose was selected keeping the rest of parameters constant. The maximum value of response variable was found to be ~99% using CFA-$CoFe_2O_4$(1:1) composite and is located somewhere in the middle of the graphs. The strong correlation suggest that the values of response variable increase considerably with the increase in the concentration of oxidant dose at optimum catalyst dose and reached maximum. However, the higher concentration above optimized one, does not support the degradation even at high oxidant and catalyst dose (Yaqubzadeh et al., 2016).

The combine effect of dye dose and H_2O_2 dose is shown in Fig. 11(b) under constant composite concentration. The 3-D contour showed that at low dye dose higher values of %age degradation was observed while increasing the H_2O_2 dose up to specific value. The 10p pm MB was degraded effectively at optimized H_2O_2 dose, while reduction in %age degradation was observed with the increase in dye dose. The reason of this could be attributed to the reason already explained in section 3.2.4.

The mutual effect of composite dose and dye concentration on %age degradation was studied at optimized oxidant dose constant and 3D and contour graphs are presented in Fig. 11(c). The increase in oxidative photocatalytic degradation potential of CFA-$CoFe_2O_4$(1:1) composite was due to the increase in the composite concentration up to specific value where it reaches a maximum at specific dye concentration.

The final equation in terms of coded factors (CFA-$CoFe_2O_4$ (1:1) for MB degradation is given as:

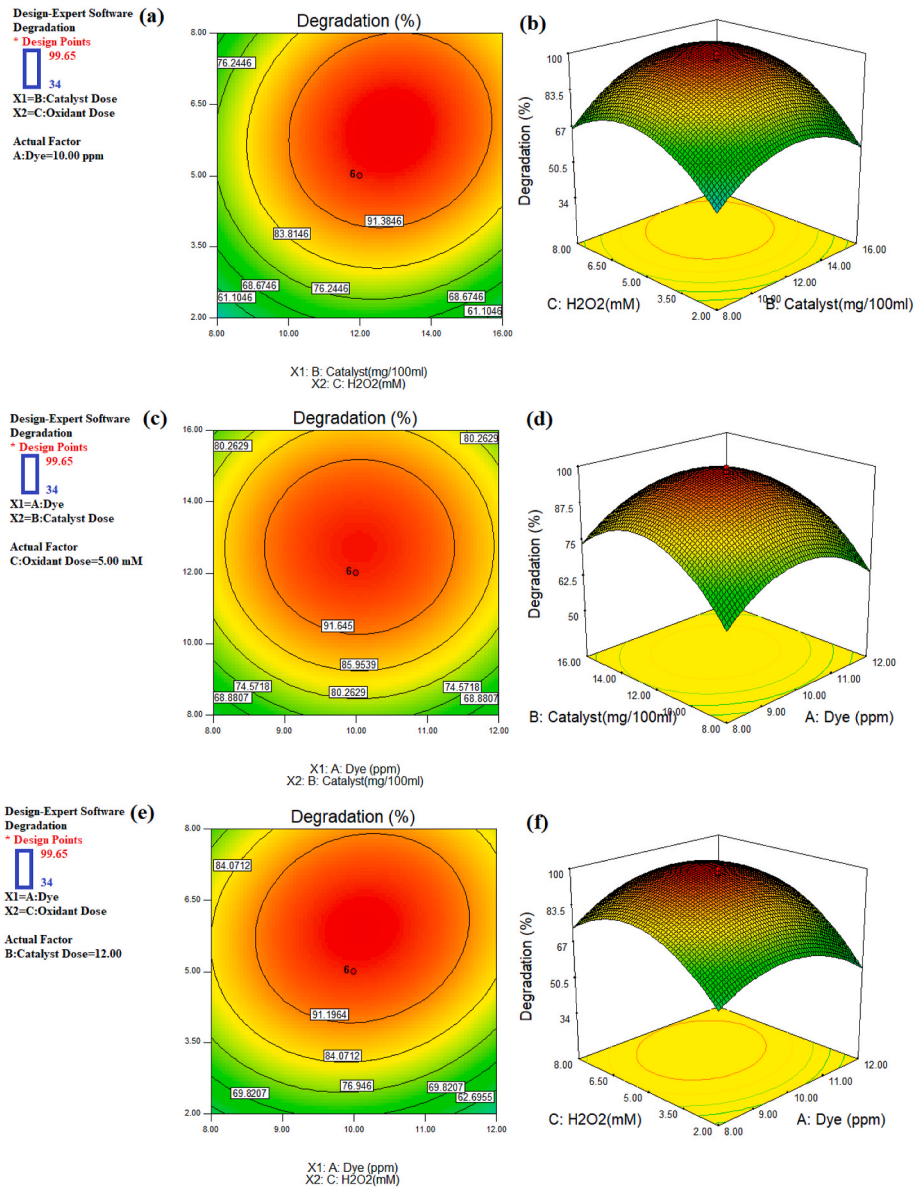

Fig. 11. Response Surfaces (right side3D surfaces, left side contour plots) showing the combined effect of (a) oxidant dose and catalyst dose, (b) dye concentration and catalyst dose, and (c) dye concentration and oxidant dose using CFA-$CoFe_2O_4$(1:1).

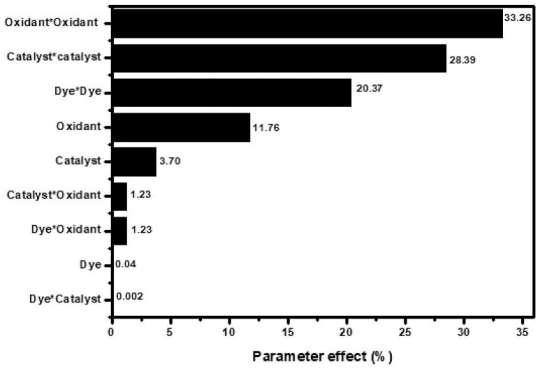

Fig. 12. Pareto analysis for various process parameters.

$$\textbf{Degradation} = +96.84 + 0.56 \times \mathbf{A} + 5.43 \times \mathbf{B} + 9.68 \times \mathbf{C} + 0.13 \times \mathbf{A} \times \mathbf{B} + 3.13 \times \mathbf{A} \times \mathbf{C} + 3.13 \times \mathbf{B} \times \mathbf{C} - 12.74 \times \mathbf{A}^2 - 15.04 \times \mathbf{B}^2 - 16.28 \times \mathbf{C}^2 \quad (21)$$

The percentage effect of regression parameters on response variable was also determined and the results are presented in the form of pareto chart (**Fig. 12**). The percentage effect of every individual parameter was calculated using the formula (Khataee et al., 2013) given below:

$$\mathbf{P_i} = \left[\frac{\mathbf{b_i^2}}{\sum \mathbf{b_i^2}}\right] \times 100 \quad \mathbf{i} \neq 0 \quad (22)$$

Here, b is the regression coefficient of the respective parameter. The results indicate that the oxidant-oxidant combination impart the most significant parameter effect (33.26) on percentage degradation of MB dye.

4. Conclusions

The pristine cobalt ferrite and its coal fly ash composite photocatalysts were synthesized using facile hydrothermal approach. All the catalysts were well characterized using FTIR, XRD, XPS, and SEM/EDS analysis. All the analysis supports the successful insertion of CFA into cobalt ferrite. The cationic dye (methylene blue) was chosen as model pollutant to consider the response of CFA composites and pristine cobalt ferrite. The result of surface charges of catalysts under acidic and basic conditions of solution pH suggest that the CFA based cobalt ferrite provide wider pH range for dye degradation as compared to pristine cobalt ferrite. The improved performance of CFA based cobalt ferrite composites is also attributed to the effective charge separations due to engineered heterojunction. The kinetic analysis revealed BMG kinetic model is the best suited for dye degradation study. Besides improved photocatalysis, the composites assure the reclamation of coal fly ash into value added products. The facile synthesis strategy and effective photocatalytic degradation potential of composite photocatalysts demonstrated that this research can be extended to modify other catalytic systems.

Credit author statement

Nimra Nadeem: Investigation, Writing – original draft preparation, Revised draft preparation. Muhammad Yaseen: Resources, Data curation. Zulfiqar Ahmad Rehan: Conceptualization, Software, Revised draft preparation. Muhammad Zahid: Supervision, Project administration, Writing – review & editing. Rana Abdul Shakoor: Formal analysis, Methodology. Asim Jillani: Formal analysis, Writing – review & editing. Javed Iqbal: Resources, Data curation. Shahid Rasul: Conceptualization, Validation. Imran Shahid: Visualization, Writing – review & editing.

Declaration of competing interest

The authors declare that they have no known competing financial interests or personal relationships that could have appeared to influence the work reported in this paper.

Acknowledgements

Dr. Muhammad Zahid (corresponding author) is thankful to TWAS (Grant No. 15-410 RG/MSN/AS_C–FR3240288961 under TWAS-COMSTECH joint Research Grant) for equipment and the University of Agriculture Faisalabad, Pakistan for facilities to conduct this research. The valuable support from Center of Nanotechnology, King Abdulaziz University, Jeddah, Saudi Arabia and Central Lab, LUMS Pakistan for characterization of samples is highly acknowledged.

Appendix A. Supplementary data

Supplementary data to this article can be found online at https://doi.org/10.1016/j.envres.2021.112280.

References

Asma, T., et al., 2019. Fe_3O_4 -GO composite as efficient heterogeneous photo-Fenton's catalyst to degrade pesticides. Mater. Res. Express 6, 015608.
Barreto, F., et al., 2016. Behavior of dihydroxybenzenes and gallic acid on the Fenton-based decolorization of dyes. Desalination Water Treat. 57, 431–439.
Chen, J., Zhu, L., 2007. UV-Fenton discolouration and mineralization of Orange II over hydroxyl-Fe-pillared bentonite. J. Photochem. Photobiol. Chem. 188, 56–64.
Choi, Y.I., et al., 2015. Recyclable magnetic $CoFe_2O_4$/BiOX (X= Cl, Br and I) microflowers for photocatalytic treatment of water contaminated with methyl orange, rhodamine B, methylene blue, and a mixed dye. RSC Adv. 5, 79624–79634.
Chu, W., et al., 2007. The effect of solution pH and peroxide in the TiO_2-induced photocatalysis of chlorinated aniline. J. Hazard Mater. 141, 86–91.
Chu, W., et al., 2004. An unconventional approach to studying the reaction kinetics of the Fenton's oxidation of 2, 4-dichlorophenoxyacetic acid. Chemosphere 57, 1165–1171.
Clara, J.J., Sugirtha, P., 2016. Study of SEM/EDXS and FTIR for fly ash to determine the chemical changes of ash in marine environment. Int. J. Sci. Res. 5, 1688–1693.
Dou, R., et al., 2020. Manganese doped magnetic cobalt ferrite nanoparticles for dye degradation via a novel heterogeneous chemical catalysis. Mater. Chem. Phys. 240, 122181.
Eghbali, P., et al., 2019. Strontium titanate nanocubes assembled on mesoporous graphitic carbon nitride (SrTiO3/mpg-C3N4): preparation, characterization and catalytic performance. J. Mol. Liq. 290, 111208.
Enesca, A., et al., 2014. Tuning SnO_2–TiO_2 tandem systems for dyes mineralization. Appl. Catal. B Environ. 147, 175–184.
Farhadi, S., et al., 2017. Ultrasound-assisted degradation of organic dyes over magnetic $CoFe_2O_4$@ZnS core-shell nanocomposite. Ultrason. Sonochem. 37, 298–309.
Gastelo, E., et al., 2019. Elimination of Escherichia coli in water using cobalt ferrite nanoparticles: laboratory and pilot plant experiments. Materials 12, 2103.
Ghanbari, F., et al., 2021a. Insights into paracetamol degradation in aqueous solutions by ultrasound-assisted heterogeneous electro-Fenton process: key operating parameters, mineralization and toxicity assessment. Separ. Purif. Technol. 266, 118533.
Ghanbari, F., et al., 2021b. Electrochemical activation of peroxides for treatment of contaminated water with landfill leachate: efficacy, toxicity and biodegradability evaluation. Chemosphere 279, 130610.
Ghanbari, F., et al., 2020. TiO2 nanoparticles removal by electrocoagulation using iron electrodes: catalytic activity of electrochemical sludge for the degradation of emerging pollutant. J. Mol. Liq. 310, 113217.
Goyal, A., et al., 2017. Augmenting the catalytic performance of spinel nanoferrites ($CoFe_2O_4$ and $NiFe_2O_4$) via incorporation of Al into the lattice. New J. Chem. 41, 8320–8332.
Guedes, A.M., et al., 2003. Fenton oxidation of cork cooking wastewater—overall kinetic analysis. Water Res. 37, 3061–3069.
Hassani, A., et al., 2018a. Heterogeneous sono-Fenton-like process using magnetic cobalt ferrite-reduced graphene oxide (CoFe2O4-rGO) nanocomposite for the removal of organic dyes from aqueous solution. Ultrason. Sonochem. 40, 841–852.
Hassani, A., et al., 2018b. Monodisperse cobalt ferrite nanoparticles assembled on mesoporous graphitic carbon nitride (CoFe2O4/mpg-C3N4): a magnetically recoverable nanocomposite for the photocatalytic degradation of organic dyes. J. Magn. Magn Mater. 456, 400–412.
Hassani, A., et al., 2020. Acetaminophen removal from aqueous solutions through peroxymonosulfate activation by CoFe2O4/mpg-C3N4 nanocomposite: insight into the performance and degradation kinetics. Environ. Technol. Innov. 20, 101127.
Hassani, A., et al., 2018c. Sonocatalytic removal of methylene blue from water solution by cobalt ferrite/mesoporous graphitic carbon nitride (CoFe 2 O 4/mpg-C 3 N 4) nanocomposites: response surface methodology approach. Environ. Sci. Pollut. Control Ser. 25, 32140–32155.
Hassani, A., et al., 2018d. Enhanced removal of basic violet 10 by heterogeneous sono-Fenton process using magnetite nanoparticles. Ultrason. Sonochem. 42, 390–402.
Hassani, A., et al., 2018e. Preparation of magnetite nanoparticles by high-energy planetary ball mill and its application for ciprofloxacin degradation through heterogeneous Fenton process. J. Environ. Manag. 211, 53–62.
He, H.Y., Lu, J., 2017. Highly photocatalytic activities of magnetically separable reduced graphene oxide-$CoFe_2O_4$ hybrid nanostructures in dye photodegradation. Separ. Purif. Technol. 172, 374–381.
Hu, L., et al., 2018. Enhanced degradation of Bisphenol A (BPA) by peroxymonosulfate with Co_3O_4-Bi_2O_3 catalyst activation: effects of pH, inorganic anions, and water matrix. Chem. Eng. J. 338, 300–310.
Huang, Y.-H., et al., 2008. Comparative study of oxidation of dye-Reactive Black B by different advanced oxidation processes: fenton, electro-Fenton and photo-Fenton. J. Hazard Mater. 154, 655–662.
Jilani, A., et al., 2020. Sulfonated polyaniline-encapsulated graphene@graphitic carbon nitride nanocomposites for significantly enhanced photocatalytic degradation of phenol: a mechanistic study. New J. Chem. 44, 19570–19580.
Khataee, A., et al., 2013. Response surface analysis of removal of a textile dye by a Turkish coal powder. Adv. Environ. Res. 2, 291–308.
Leifeld, V., et al., 2018. Ferrous ions reused as catalysts in Fenton-like reactions for remediation of agro-food industrial wastewater. J. Environ. Manag. 222, 284–292.
Malik, P., Saha, S., 2003. Oxidation of direct dyes with hydrogen peroxide using ferrous ion as catalyst. Separ. Purif. Technol. 31, 241–250.
Messele, S., et al., 2018. Zero-valent iron supported on nitrogen-doped carbon xerogel as catalysts for the oxidation of phenol by fenton-like system. Environ. Technol. 39, 2951–2958.
Motlagh, P.Y., et al., 2020. ZnFe-LDH/GO nanocomposite coated on the glass support as a highly efficient catalyst for visible light photodegradation of an emerging pollutant. J. Mol. Liq. 302, 112532.
Moura, M.N., et al., 2017. Synthesis, characterization and photocatalytic properties of nanostructured $CoFe_2O_4$ recycled from spent Li-ion batteries. Chemosphere 182, 339–347.
Mozgawa, W., et al., 2014. Investigation of the coal fly ashes using IR spectroscopy. Spectrochim. Acta Mol. Biomol. Spectrosc. 132, 889–894.
Mushtaq, F., et al., 2019. Possible applications of coal fly ash in wastewater treatment. J. Environ. Manag. 240, 27–46.
Mushtaq, F., et al., 2020. $MnFe_2O_4$/coal fly ash nanocomposite: a novel sunlight-active magnetic photocatalyst for dye degradation. Int. J. Environ. Sci. Technol. 17, 4233–4248.
Nadeem, N., et al., 2021a. Coal fly ash-based copper ferrite nanocomposites as potential heterogeneous photocatalysts for wastewater remediation. Appl. Surf. Sci. 565, 150542.
Nadeem, N., et al., 2021b. Wastewater Remediation Using Coal Fly Ash Nanocomposites. Aquananotechnology. Elsevier, pp. 149–174.

Nadeem, N., et al., 2021c. Improved photocatalytic degradation of dye using coal fly ash-based zinc ferrite (CFA/ZnFe2O4) composite. Int. J. Environ. Sci. Technol.
Nadeem, N., et al., 2020. Degradation of reactive dye using heterogeneous photo-Fenton catalysts: ZnFe2O4 and GO-ZnFe2O4 composite. Mater. Res. Express 7, 015519.
Naushad, M., et al., 2019. Photodegradation of toxic dye using Gum Arabic-crosslinked-poly (acrylamide)/Ni (OH) 2/FeOOH nanocomposites hydrogel. J. Clean. Prod. 241, 118263.
Nidheesh, P.V., et al., 2013. Degradation of dyes from aqueous solution by Fenton processes: a review. Environ. Sci. Pollut. Control Ser. 20, 2099–2132.
Radjenovic, J., Sedlak, D.L., 2015. Challenges and opportunities for electrochemical processes as next-generation technologies for the treatment of contaminated water. Environ. Sci. Technol. 49, 11292–11302.
Rahman, M.U., et al., 2021. Solar driven photocatalytic degradation potential of novel graphitic carbon nitride based nano zero-valent iron doped bismuth ferrite ternary composite. Opt. Mater. 120, 111408.
Rubab, M., et al., 2021. Synthesis and photocatalytic degradation of rhodamine B using ternary zeolite/WO3/Fe3O4 composite. Nanotechnology 32, 345705.
Saher, R., et al., 2021. Sunlight-driven photocatalytic degradation of rhodamine B dye by Ag/FeWO4/g-C3N4 composites. Int. J. Environ. Sci. Technol. 18, 927–938.
Santana, C.S., Aguiar, A., 2015. Effect of biological mediator, 3-hydroxyanthranilic acid, in dye decolorization by Fenton processes. Int. Biodeterior. Biodegrad. 104, 1–7.
Shaban, M., et al., 2018a. Recycling of glass in synthesis of MCM-48 mesoporous silica as catalyst support for Ni_2O_3 photocatalyst for Congo red dye removal. Clean Technol. Environ. Policy 20, 13–28.
Shaban, M., et al., 2017. Photocatalytic removal of Congo red dye using MCM-48/Ni_2O_3 composite synthesized based on silica gel extracted from rice husk ash; fabrication and application. J. Environ. Manag. 204, 189–199.
Shaban, M., et al., 2018b. TiO_2 nanoribbons/carbon nanotubes composite with enhanced photocatalytic activity; fabrication, characterization, and application. Sci. Rep. 8, 1–17.
Shao, P., et al., 2017. Heterogeneous activation of peroxymonosulfate by amorphous boron for degradation of bisphenol S. J. Hazard Mater. 322, 532–539.
Shao, P., et al., 2018. Identification and regulation of active sites on nanodiamonds: establishing a highly efficient catalytic system for oxidation of organic contaminants. Adv. Funct. Mater. 28, 1705295.
Shao, P., et al., 2020. Potential Difference Driving Electron Transfer via Defective Carbon Nanotube towards Selective Oxidation of Organic Micro-pollutants. Environmental Science & Technology.
Sharma, D., Satyanarayana, T., 2006. A marked enhancement in the production of a highly alkaline and thermostable pectinase by Bacillus pumilus dcsr1 in submerged fermentation by using statistical methods. Bioresour. Technol. 97, 727–733.
Sharma, G., et al., 2018. Facile fabrication of $Zr_2Ni_1Cu_7$ trimetallic nano-alloy and its composite with Si_3N_4 for visible light assisted photodegradation of methylene blue. J. Mol. Liq. 272, 170–179.
Tabasum, A., et al., 2021a. UV-accelerated photocatalytic degradation of pesticide over magnetite and cobalt ferrite decorated graphene oxide composite. Plants 10, 6.
Tabasum, A., et al., 2021b. UV-accelerated photocatalytic degradation of pesticide over magnetite and cobalt ferrite decorated graphene oxide composite. Plants 10, 6.
Tabasum, A., et al., 2020. Degradation of acetamiprid using graphene-oxide-based metal (Mn and Ni) ferrites as Fenton-like photocatalysts. Water Sci. Technol. 81, 178–189.
Venkatakrishnan, A., Kuppa, V.K., 2018. Polymer adsorption on rough surfaces. Curr. Opinion Chem. Eng. 19, 170–177.
Visa, M., et al., 2015. Tungsten oxide – fly ash oxide composites in adsorption and photocatalysis. J. Hazard Mater. 289, 244–256.
Wang, N., et al., 2018. Adsorptive removal of organics from aqueous phase by acid-activated coal fly ash: preparation, adsorption, and Fenton regenerative valorization of “spent” adsorbent. Environ. Sci. Pollut. Control Ser. 25, 12481–12490.
Wang, N., et al., 2019. Degradation of Acid Organic 7 by modified coal fly ash-catalyzed Fenton-like process: kinetics and mechanism study. Int. J. Environ. Sci. Technol. 16, 89–100.
Wang, N., et al., 2021. Treatment of polymer-flooding wastewater by a modified coal fly ash-catalysed Fenton-like process with microwave pre-enhancement: system parameters, kinetics, and proposed mechanism. Chem. Eng. J. 406, 126734.
Wang, N., et al., 2020. Leachability and adverse effects of coal fly ash: a review. J. Hazard Mater. 396, 122725.
Wang, S., Lu, G., 2007. Effect of chemical treatment on Ni/fly-ash catalysts in methane reforming with carbon dioxide. Studies in Surface Science and Catalysis. Elsevier, pp. 275–280.
Xu, H.-Y., et al., 2018. Nanoparticles of magnetite anchored onto few-layer graphene: a highly efficient Fenton-like nanocomposite catalyst. J. Colloid Interface Sci. 532, 161–170.
Yao, Z., et al., 2015. A comprehensive review on the applications of coal fly ash. Earth Sci. Rev. 141, 105–121.
Yaqubzadeh, A., et al., 2016. Low-cost preparation of silica aerogel for optimized adsorptive removal of naphthalene from aqueous solution with central composite design (CCD). J. Non-Cryst. Solids 447, 307–314.
Zahid, M., et al., 2019. Metal Ferrites and Their Graphene-Based Nanocomposites: Synthesis, Characterization, and Applications in Wastewater Treatment. Magnetic nanostructures. Springer, pp. 181–212.
Zahid, M., et al., 2020. Hybrid nanomaterials for water purification. Multifunctional Hybrid Nanomaterials for Sustainable Agri-Food and Ecosystems. Elsevier, pp. 155–188.
Zhao, G., et al., 2005. Synthesis and characterization of Prussian blue modified magnetite nanoparticles and its application to the electrocatalytic reduction of H_2O_2. Chem. Mater. 17, 3154–3159.
Zuorro, A., Lavecchia, R., 2014. Evaluation of UV/H_2O_2 advanced oxidation process (AOP) for the degradation of diazo dye Reactive Green 19 in aqueous solution. Desalination Water Treat. 52, 1571–1577.